Simulation of Semiconductor Processes and Devices 2016
Edited by E. Bär, J. Lorenz, and P. Pichler

A 2D Axisymmetric Dynamic Drift-Diffusion Model for Numerical Simulation of Resistive Switching Phenomena in Metal Oxides

A. Marchewka
Institut für Werkstoffe der Elektrotechnik II
RWTH Aachen University
52074 Aachen, Germany
marchewka@iwe.rwth-aachen.de

R. Waser and S. Menzel
Peter Grünberg Institut
Forschungszentrum Jülich
52425 Jülich, Germany

***Abstract*— We present a 2D axisymmetric model to simulate nonisothermal electronic-ionic transport in resistive-switching metal-oxide-metal structures, taking into account the effect of contact potential barriers. The model is applied to study the reset process in terms of the dynamic equilibrium between ionic drift and diffusion and of the physical parameters influencing this equilibrium. Furthermore, it is shown to capture the typical abrupt set and gradual reset behavior occurring during quasi-static voltage sweeps. Analyses of the filament evolution during the voltage sweep are performed to characterize the resulting resistance states.**

Keywords—ReRAM, Schottky contact, gradual reset, filament, simulation model

I. Introduction

Resistively switching metal-oxide-metal structures based on the valence-change mechanism have generated broad interest for their potential application as memory or logic devices in future nanoelectronics [1]. They exhibit bipolar switching with the set and reset operation occurring at opposite voltage polarities. Their *I–V* characteristics are characterized by an abrupt set transition from the high resistive state (HRS) to the low resistive state (LRS) and a gradual reset transition from the LRS to the HRS. There exists broad consensus that the switching mechanism relies on temperature- and field-accelerated migration of donors inside the oxide and an associated change in the electronic barrier at the metal-oxide interface [1]. The donor redistribution is often interpreted in terms of formation and dissolution of a conductive filament [2,3]. Despite recent rapid progress in the field of resistive switching, a profound understanding of the underlying physics is still missing. This fact is closely linked to the lack of comprehensive physical models including all relevant aspects. In this work, we present such a model that combines coupled ionic-electronic transport in the oxide with Joule heating and a Schottky-barrier transport model in a 2D axisymmetric domain. This approach has recently been used to study the reset dynamics of TaO_x-based resistive switches, revealing that the gradual nature of the reset process can be attributed to interacting ionic drift and diffusion processes approaching equilibrium [4]. Here, we employ this model for an in-depth study of the transient reset process and the characterization of quasi-static *I–V* sweeps, which are further discussed in terms of conductive filament evolution.

II. Simulation Model

We consider an axisymmetric representation (radial coordinate r, axial coordinate z, radius $R = 100$ nm) of a metal-oxide-metal device consisting of a 75 nm thick substrate, a 25 nm thick bottom electrode (BE), a donor-doped oxide layer of thickness L, and a 5 nm thick top electrode (TE) with a 25 nm thick Pt capping layer. In the initial state, a conductive filament characterized by enhanced donor concentration inside a radius $r \le r_{\mathrm{fil}} = 10$ nm is assumed to be present inside the oxide. A Schottky-like contact of a high barrier $e\phi_{\mathrm{Bn0}}(r \le r_{\mathrm{fil}},0)$ is assumed at the BE/oxide interface ($z = 0$), and an ohmic-like contact of a low barrier $e\phi_{\mathrm{Bn0}}(r \le r_{\mathrm{fil}},L)$ is assumed at the TE/oxide interface ($z = L$) in the filamentary region. Outside the filament region, the current flow is assumed to be suppressed, therefore large barriers $e\phi_{\mathrm{Bn0}}(r > r_{\mathrm{fil}},0)$ and $e\phi_{\mathrm{Bn0}}(r > r_{\mathrm{fil}},L)$ apply. The calculation of the transient currents and quasi-static *I–V* characteristics is performed by solving a set of six partial differential equations. First, the heat equation

$$-\nabla\left(\kappa\nabla T\right) = JF, \tag{1}$$

the Poisson equation

$$\nabla\left(\varepsilon\nabla\psi\right) = e\left(n - N_{\mathrm{VO}}^{+} - 2N_{\mathrm{VO}}^{2+}\right), \tag{2}$$

and the drift-diffusion equation for electrons

$$\nabla\left(\mu_n n\nabla\psi - D_n\nabla n - nD_{\mathrm{T},n}\nabla T\right) = \pm\frac{1}{e}\frac{\partial J_{\mathrm{tun}}}{\partial z} \tag{3}$$

are solved for self-consistently in an inner Gummel loop. While the heat equation is solved in the entire computational domain, equations (2) and (3) are only solved inside the oxide layer. In the above equations, κ is the thermal conductivity, T the temperature, F the electric field, J the total current density, ε the permittivity of the oxide, ψ the potential, n the electron concentration, N_{VO}^{+} (N_{VO}^{2+}) the concentration of the singly (doubly) ionized donor-type oxygen vacancies, μ_n the electron

978-1-5090-0818-6/16/$31.00 ©2016 IEEE

mobility, D_n the electron diffusion coefficient, and $D_{T,n}$ the thermal diffusion coefficient for electrons. The term on the right-hand side of (3) describes a local generation/recombination rate due to electron tunneling through the contact potential barrier. The tunneling current density J_{tun} is given as

$$J_{\text{tun}}(z) = \frac{A^* T}{k_B} \int_{E_{C,\min}(z)}^{E_{C,\max}(z)} \mathcal{T} \quad {}_{\text{upply}}(E_z)\, dE_z, \tag{4}$$

with the Richardson constant A^*, the Boltzmann constant k_B, the transmission coefficient $\mathcal{T}(E_z)$, and the supply function $N_{\text{supply}}(E_z)$. The integration is performed over the local conduction-band energy (E_C) difference across the control volume of the discretized domain. The thermionic-emission current density across the metal-oxide interface $z_i = \{0, L\}$ serves as a boundary condition for (3) and is calculated as

$$J_{\text{TE}}(z_i) = \frac{A^* T}{k_B} \int_{E_C(z_i)}^{\infty} N_{\text{supply}}(E_z)\, dE_z. \tag{5}$$

The boundary conditions for the potential in (2) are expressed in terms of the barrier heights at the contacts according to

$$\psi(0) = \psi_i^0 + \frac{k_B T}{e}\eta_{\text{Fn}}^0 - \phi_{\text{Bn}}(0) + V_a - V_{\text{RS}}, \tag{6}$$

$$\psi(L) = \psi_i^0 + \frac{k_B T}{e}\eta_{\text{Fn}}^0 - \phi_{\text{Bn}}(L), \tag{7}$$

with ψ_i^0 being the intrinsic potential, η_{Fn}^0 the energy difference between the bottom of the conduction band and the Fermi level, normed by $k_B T/e$, $\phi_{\text{Bn}}(z_i)$ the effective potential barrier height at the contact, V_a the applied voltage and V_{RS} the voltage drop across a series resistance R_{series}. At the radial boundary $r = R$, homogeneous Neumann conditions are applied to the Poisson equation (2) and the electron drift-diffusion equation (3). For the heat equation (1), constant-temperature boundary conditions ($T = 300$ K) apply at the top and the bottom side of the geometry and at $r = R$. Further, axial symmetry implies homogeneous Neumann boundary conditions at $r = 0$ for all dependent variables in the system of equations.

With the new values for ψ and T obtained by solving (1) to (3) using the boundary conditions described above, the drift-diffusion equation for the doubly ionized oxygen-vacancies

$$\frac{\partial N_{\text{VO}}^{2+}}{\partial t} - \nabla\left(\mu_{\text{VO}} N_{\text{VO}}^{2+} \nabla\psi + D_{\text{VO}} \nabla N_{\text{VO}}^{2+} + N_{\text{VO}}^{2+} D_{\text{T,VO}} \nabla T\right) = -R_{\text{VO,2}}, \tag{8}$$

is solved for a given time step, assuming the ionic current density to vanish at the domain boundaries. The rate equations

$$\frac{\partial N_{\text{VO}}^{+}}{\partial t} = -R_{\text{VO,1}}, \tag{9}$$

$$\frac{\partial N_{\text{VO}}^{0}}{\partial t} = -R_{\text{VO,0}}. \tag{10}$$

for the singly and neutral oxygen vacancies, which are both considered immobile, are solved for the same time step. In (8) to (10), μ_{VO} is the oxygen-vacancy mobility, D_{VO} ($D_{\text{T,VO}}$) the oxygen-vacancy (thermal) diffusion coefficient, and $R_{\text{VO,2}}$, $R_{\text{VO,1}}$, and $R_{\text{VO,0}}$ represent recombination rates derived from the laws of mass action for the ionization reactions along with the dopant ionization statistics [4]. The mobility μ_i and diffusion coefficient D_i, $i = \{n, \text{VO}\}$, are assumed to be related to each other by the Einstein relation, and the thermal diffusion coefficient $D_{T,i}$ is expressed in terms of D_i and the temperature-dependent Soret coefficient $S_{T,i}$ as $D_{T,i} = S_{T,i} D_i$. The donor diffusion is assumed to be temperature activated with

$$D_{\text{VO}} = D_0 \exp\left(-\frac{\Delta H_{\text{D,VO}}}{k_B T}\right)\left(1 - \frac{N_{\text{VO}}^{2+}}{N_{\text{VO,max}}}\right), \tag{11}$$

where D_0 is the diffusion-coefficient prefactor, $\Delta H_{\text{D,VO}}$ is the migration enthalpy, and $N_{\text{VO,max}}$ is the maximum possible donor concentration in the oxide layer.

III. Simulation Results

A. Reset pulse studies of the dynamic equilibrium state

The model outlined in section II has recently been used to analyze the reset kinetics of TaO_x-based nanocrossbar devices during 1 µs voltage pulses [4]. The results therein suggest that an equilibrium state between ionic drift and diffusion is approached, but not completely reached within the applied pulse duration. Here, we characterize the equilibrium state by performing simulations with longer reset pulse durations using the same material parameter settings as in [4]. Fig. 1(a) shows the transient currents upon pulse amplitudes of $V_a = V_{\text{pulse}} = 1.3$ V, 1.4 V, 1.5 V, and 1.6 V. They have been simulated until they reach a plateau suggesting that equilibrium is established. Higher equilibrium currents I_∞ are observed for larger voltages and the corresponding resistance values $R = V_{\text{pulse}}/I_\infty$ decrease. Maps of the donor distribution in equilibrium state are given in Fig. 1(b). The distributions and filament shapes are similar for the different V_{pulse}. The concentration gradient along the z-axis is a little less steep for larger voltages, since the higher current implies higher temperatures and enhanced diffusion, driving the donors back towards the Schottky-like electrode. In terms of filament evolution, this trend implies slightly smaller depleted gaps between the electrode and the filament, leading to smaller HRS resistances for larger pulse voltages. As shown in numerous experiments [4-6], different high-resistance states can be programmed using quasi-static I–V sweeps with varying reset stop voltage. In these measurements, the resistance values increase with increasing reset voltage, indicating that equilibrium does not prevail in this voltage range.

The influence of ambient temperature T_a, donor migration enthalpy ΔH_D, and donor ionization energies $\Delta E_{\text{VO}}^{\times\rightarrow 1}$ and $\Delta E_{\text{VO}}^{1\rightarrow 2}$ on the reset currents I_0 and I_∞ and the time needed to establish equilibrium are investigated. The latter can be characterized in terms of a point P_5 on the I–t curve and the corresponding time τ_5 that is needed for a current decrease to 5 % of the total decrease $\Delta I = I_0 - I_\infty$ as indicated in the inset of Fig. 1(a). Fig. 2(a) and (b) display the currents I_0 and I_∞ and the decay time τ_5 for ambient temperatures T_a varied from 275 K to 350 K for the four pulse voltages $V_{\text{pulse}} = 1.3$ V, 1.4 V, 1.5 V,

978-1-5090-0818-6/16/$31.00 ©2016 IEEE

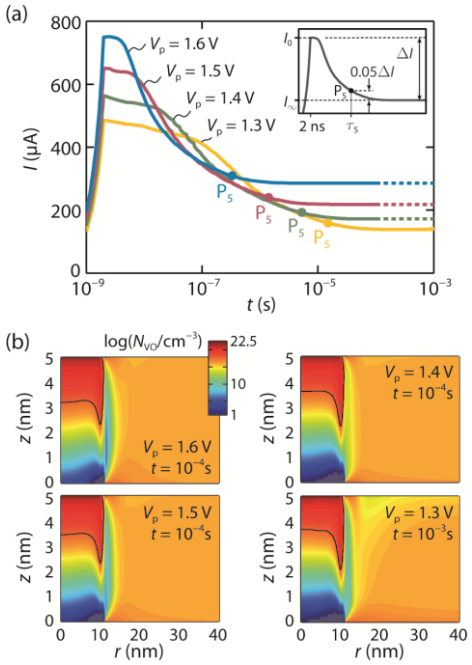

(a) Simulated transient currents for four different pulse voltages at an ambient temperature T_a = 300 K, a donor migration enthalpy of ΔH_D = 0.8 eV, and an ionization energy of $\Delta E_{VO}^{\times\to1} = \Delta E_{VO}^{1\to2}$ = 3 meV. The dashed lines are extrapolations to larger times. The inset shows the definition of the currents I_0 and I_∞ and the decay time τ_5. (b) Maps of donor distribution in equilibrium state at the end of the voltage pulse with the black isoline of $N_{VO} = 6.4\times10^{17}$ cm^{-3} illustrating the evolution of the filament.

and 1.6 V. Both I_0 and I_∞ slightly increase with increasing temperature as the thermionic emission of electrons across the Schottky-like barrier into the oxide layer is thermally enhanced. The decay time τ_5 decreases nearly exponentially with increasing temperature by approximately one order of magnitude per 50 K. This behaviour is primarily caused by the temperature-activated increase of donor mobility according to (11). Similarly, changing the donor migration enthalpy ΔH_D can be expected to have a strong impact on the reset dynamics due to the exponential impact on the mobility. The dependence of I_0 and I_∞ as well as of τ_5 on ΔH_D is given in Fig. 2(c) and (d) for the same four pulse voltages, with ΔH_D assuming values between 0.5 eV and 0.8 eV. Since ΔH_D is not directly related to the electrical conductivity, a variation of ΔH_D hardly changes the reset currents I_0 and I_∞. The decay time τ_5, in contrast, is primarily determined by the donor mobility, and exhibits an increase of more than one order of magnitude per 0.1 eV increase in ΔH_D. The influence of different donor ionization energies on the reset currents I_0 and I_∞ and the decay time τ_5 is shown in Fig. 2(e) and (f) with V_{pulse} = 1.3 V, 1.4 V, 1.5 V, and 1.6 V as the parameter. Here, $\Delta E_{VO}^{\times\to1}$ and $\Delta E_{VO}^{1\to2}$ are equal to each other and are varied simultaneously between 3 meV and 125 meV. The currents I_0 and I_∞ both decrease with increasing ionization energy, because the higher ionization energy results in a lower electron concentration and therefore lower currents. The effect on I_0 is stronger compared to the one on I_∞, and thus the window between both current levels declines, implying a reduced HRS-to-LRS resistance ratio. The decay time τ_5 increases nonlinearly with increasing values of

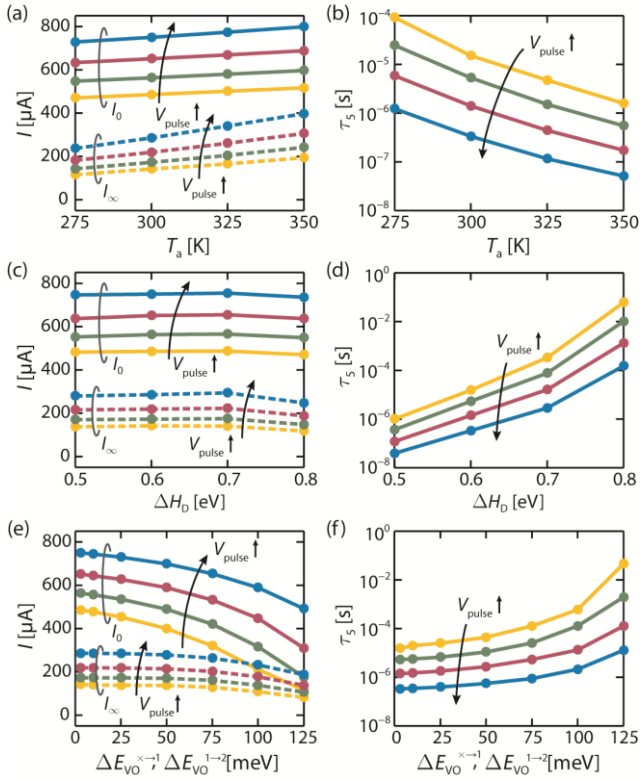

Fig. 2. Influence of ambient temperature T_a on (a) the currents I_0 and I_∞, and (b) the decay time τ_5; influence of donor migration enthalpy ΔH_D on (c) the currents I_0 and I_∞, and (d) the decay time τ_5; influence of donor ionization energies $\Delta E_{VO}^{\times\to1}$ and $\Delta E_{VO}^{1\to2}$ on the (e) the currents I_0 and I_∞, and (f) the decay time τ_5.

$\Delta E_{VO}^{\times\to1}$ and $\Delta E_{VO}^{1\to2}$, showing to up to 3 orders of difference between the lowest and the highest ionization energy. The impact of the donor ionization on the reset dynamics is complex. Via its direct relation to the electron concentration, it affects the currents and therefore the temperature in the oxide, which itself determines the donor mobility as explained above. Additionally, the donor ionization energy has a direct impact on the number of mobile donors available, i. e. doubly ionized ones, and it thus influences the donor profiles e during the reset process. For larger ionization energies, less donors are doubly ionized, resulting in a deceleration of the reset process.

B. Filament evolution during quasi-static I–V sweeps

Quasi-static current-voltage characteristics are simulated for a voltage sweep rate of 2 V/s and 10 V/s and shown in Fig. 3(a). Unlike in the simulations of the reset process, image-force-induced barrier lowering is taken into account as outlined in [7]. Parameters used for the simulations of the *I–V* curves are given in Tab. 1. Missing values were taken to be the same as in [4]. The sweeps with peak amplitudes of –1.1 V and 1.6 V start with the negative voltage polarity. The initial donor distributions were obtained by starting from a homogeneous distribution $N_{VO,fil} = 1\times10^{21}$ cm^{-3} in the filament and $N_{VO,mat} = 1\times10^{16}$ cm^{-3} in the surrounding matrix and calculating a first positive half-sweep that ends up in the HRS. The simulated *I–V* curves in Fig. 3(a) exhibit bipolar switching with an abrupt set and a gradual reset transition. With decreasing sweep rate, i. e. increasing sweep duration, the onset of the set

and reset transition shifts to lower absolute voltages, because the donors can move a larger distance during the same voltage increment at a certain temperature. The change in switching voltage is much more pronounced for the set process, since the HRS resulting from the previous reset transition is also strongly determined by the sweep rate. The currents of the HRS are lower for larger sweep rates. The corresponding donor distribution shows a larger depleted gap in front of the Schottky-like contact for larger sweep rates, because the lower sweeping time restrains donor diffusion back towards the Schottky-like contact on the falling voltage edge after the reset. A similar dependence of the set voltage on the previous reset process resulting in varying initial conditions for the set process has been observed in experiments [8]. Here, a higher reset pulse voltage results in larger set times for the same set voltage, i. e. decreased switching speed, which is argued to be due to a larger donor-depleted gap at the Schottky-like contact.

The donor redistribution during the sweep of 10 V/s is displayed in Fig. 3(b), where the eight concentration maps correspond to the donor distributions at points A to H marked in the *I–V* characteristic in Fig. 3(a). At the beginning of the sweep, the cell is in the HRS (A). The donors are piled up at the ohmic-like interface at $z = L$ and a depleted gap is present in front of the Schottky-like interface at $z = 0$. When a negative voltage is applied, they start moving towards the Schottky-like interface and the depleted gap is reduced (B). After the set process (C), the donors have accumulated at the Schottky-like contact, resulting in the LRS. When the voltage is swept back to zero, a minor part diffuses back to the ohmic-like interface as the counterforce of the drift decreases (D). During the application of the subsequent positive voltage, the electric field drives the donors again to the ohmic-like interface. Before the onset of the reset transition, most donors are still present at the Schottky-like interface (E). During reset, the donor distribution in the filament assumes a rather homogeneous intermediate state (F) and is then slowly set back to the HRS with strong accumulation at the ohmic-like interface at the peak voltage amplitude of 1.6 V (G). When decreasing the voltage again, the built-up concentration gradient is slightly decreased due to the reduced drift force (H). The resulting final donor distribution at $V = 0$ V is then very similar to the starting distribution.

TABLE I. PARAMETERS FOR SIMULATION OF THE *I–V* CURVES

Symbol	Value	Symbol	Value
L	10 nm	$e\phi_{Bn0}(r \le r_{fil},0)$	0.7 eV
ε_r	20	$e\phi_{Bn0}(r \le r_{fil},0)$	1.8 eV
ε_{opt}	5.5	$e\phi_{Bn0}(r \le r_{fil},0)$	0.1 eV
ΔE_g	3.3 eV	$e\phi_{Bn0}(r \le r_{fil},0)$	0.8 eV
$\Delta E_{VO}^{x\to1}$	3 meV	$N_{VO,max}$	5×10^{22} cm^{-3}
$\Delta E_{VO}^{1\to2}$	30 meV	μ_n	5.5 cm^2 (Vs)$^{-1}$
D_0	1×10^{-4} m^{2}s^{-1}	κ_{oxide}	5 W (mK)$^{-1}$
$\Delta H_{D,VO}$	0.8 eV	R_{series}	500 Ω

IV. CONCLUSION

In summary, an advanced dynamic numerical model is presented that includes all main physical mechanisms involved in resistive switching. Based on a 2D axisymmetric formulation of the underlying differential equations, it allows for studying the key features of resistively switching devices in terms of conductive filament evolution, offering new insights into the underlying physics.

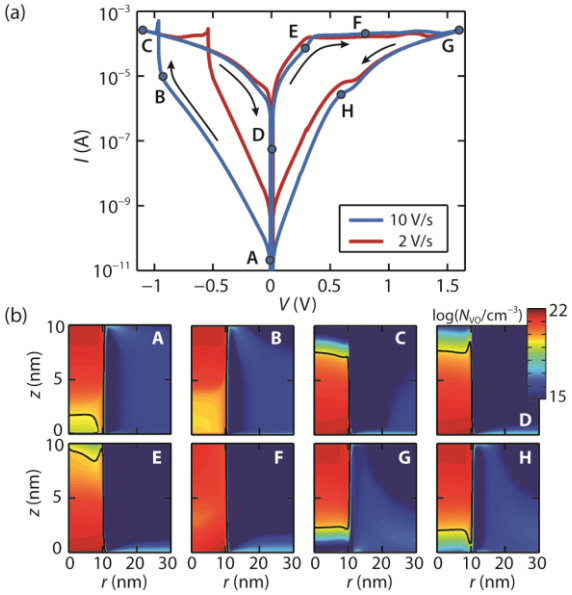

Fig. 3. (a) Simulated quasi-static *I–V* characteristics for sweep rates of 2 V/s and 10 V/s, (b) maps of donor concentration showing the redistribution of donors during the sweep of 10 V/s at points A to H as marked in (a). The black isoline of $N_{VO} = 3.2\times10^{19}$ cm^{-3} (100 oxygen vacancies inside the filament) serves to illustrate the evolution of the filament.

ACKNOWLEDGMENT

This work was supported in parts by the Deutsche Forschungsgemeinschaft (SFB 917).

REFERENCES

[1] R. Waser, R. Dittmann, G. Staikov and K. Szot, "Redox-Based Resistive Switching Memories - Nanoionic Mechanisms, Prospects, and Challenges," *Adv. Mater.*, vol. 21, pp. 2632-2663, 2009.

[2] J. J. Yang, M. D. Pickett, X. Li, D. A. A. Ohlberg, D. R. Stewart and R. S. Williams, "Memristive switching mechanism for metal/oxide/ metal nanodevices," *Nat. Nanotechnol.*, vol. 3, pp. 429-433, 2008.

[3] U. Celano, L. Goux, R. Degraeve, A. Fantini, O. Richard, H. Bender, M. Jurczak and W. Vandervorst, "Imaging the Three-Dimensional Conductive Channel in Filamentary-Based Oxide Resistive Switching Memory," *Nano Letters*, vol. 15, pp. 7970-7975, 2015.

[4] A. Marchewka, B. Roesgen, K. Skaja, H. Du, C. L. Jia, J. Mayer, V. Rana, R. Waser and S. Menzel, "Nanoionic Resistive Switching Memories: On the Physical Nature of the Dynamic Reset Process," *Adv. Electron. Mater.*, vol. 2, pp. 1500233, 2016.

[5] F. Yuan, Z. Zhang, L. Pan and J. Xu, "A Combined Modulation of Set Current With Reset Voltage to Achieve 2-bit/cell Performance for Filament-Based RRAM," *IEEE J. Electron Devices Soc.*, vol. 2, pp. 154-157, 2014.

[6] W. Kim, S. Menzel, D. J. Wouters, B. Rösgen, J. Robertson, R. Waser and V. Rana, "Impact of oxygen exchange reaction at the ohmic interface in Ta_2O_5-based ReRAM devices," submitted to *Nanoscale*, 2016.

[7] A. Marchewka, R. Waser and S. Menzel, "Physical Simulation of Dynamic Resistive Switching in Metal Oxides Using a Schottky Contact Barrier Model," *International Conference On Simulation of Semiconductor Processes and Devices (SISPAD)*, pp. 297-300, 2015.

[8] Y. Nishi, K. Fleck, U. Boettger, R. Waser and S. Menzel, "Effect of RESET Voltage on Distribution of SET Switching Time of Bipolar Resistive Switching in a Tantalum Oxide Thin Film," *IEEE Trans. Electron Devices*, vol. 62, pp. 1561-1567, 2015.